J Eng Math
DOI 10.1007/s10665-011-9482-4

Thin film dynamics on a prolate spheroid with application to the cornea

R. J. Braun · R. Usha · G. B. McFadden · T. A. Driscoll · L. P. Cook · P. E. King-Smith

Received: 23 February 2010 / Accepted: 16 May 2011

Abstract The tear film on the front of the eye is critical to proper eyesight; in many mathematical models of the tear film, the tear film is assumed to be on a flat substrate. We re-examine this assumption by studying the effect of a substrate which is representative of the human cornea. We study the flow of a thin fluid film on a prolate spheroid which is a good approximation to the shape of the human cornea. Two lubrication models for the dynamics of the film are studied in prolate spheroidal coordinates which are appropriate for this situation. One is a self-consistent leading-order hyperbolic partial differential equation (PDE) valid for relatively large substrate curvature; the other retains the next higher-order terms resulting in a fourth-order parabolic PDE for the film dynamics. The former is studied for both Newtonian and Ellis (shear thinning) fluids; for typical tear film parameter values, the shear thinning is too small to be significant in this model. For larger shear thinning, we find a significant effect on finite-time singularities. The second model is studied for a Newtonian fluid and allows for a meniscus at one end of the domain. We do not find a strong effect on the thinning rate at the center of the cornea. We conclude that the corneal shape does not have a significant effect on the thinning rate of the tear film for typical conditions.

Keywords Cornea · Curved substrate · Lubrication theory · Tear film · Thin film flow

R. J. Braun (✉) · T. A. Driscoll · L. P. Cook
Department of Mathematical Sciences, University of Delaware, Newark, DE 19716, USA
e-mail: braun@math.udel.edu

R. Usha
Department of Mathematics, Indian Institute of Technology Madras, Chennai 600 036, India

G. B. McFadden
Mathematical and Computational Sciences Division, National Institute of Standards and Technology, Gaithersburg, MD 20899-8910, USA

P. E. King-Smith
College of Optometry, The Ohio State University, Columbus, OH 43210-1280, USA

Published online: 09 June 2011

1 Introduction

The tear film on the eye is critical to proper eye health and function. It helps in protecting the eye surface with moisture, in transporting waste off the eye surface, and in providing a smooth optical surface when it is functioning properly [1]. The tear film is a multilayer film [2,3] with an outermost layer of lipids [4–6] floating upon a primarily aqueous layer [1] which in turn is on a mucin-rich region at the corneal surface (e.g., [7–9]). The precorneal tear film is a few microns thick in the center of the cornea after a blink (e.g., [10–12]) and has a considerably larger meniscus around the eye lid margins [13–15]. Tear fluid (a sample combining all components of tears) is mildly shear thinning [16] but weakly elastic [17]; recent measurements of meibomian lipids alone show that they may have significant elasticity [18], but its contribution to the overall rheology and properties of tears is yet to be understood. Other interfacial properties, such as the apparent surface tension of the tear–air interface, are definitely affected by polar lipids that are attracted to the lipid–aqueous interface [19,20], and those lipids can cause upward motion of the tear fluid after a blink [21,22]. However, the apparent surface tension of tears appears to be affected by more than the presence of polar lipids [23,24].

The tear film is commonly assumed to be Newtonian fluid in theoretical models though some shear thinning fluids have been considered [25–28]. Mathematical models for the tear film have incorporated a variety of important effects that occur in the tear film: surface tension [29–32]; polar lipid surface concentration gradients causing the Marangoni effect [21,33–35]; evaporation [6,36,37]; wettability of the corneal surface [25,26,37,38]; motion of the eye lids in one dimension [28,33,34,39–41]; and the shape of the eye opening [42,43]. While these effects may all contribute in different regions of the eye and at different times in the blink cycle, in this article, we consider a simplified model with surface tension, viscosity, and the shape of the substrate (corneal surface) only, to better understand the importance of the corneal shape in tear film dynamics.

Many articles neglect any effect of the curvature of the cornea when studying tear film dynamics based on the discussion in Berger and Corrsin [21], which in turn cites Berger's thesis [44]; however, the justification is based on the assumed *spherical* curvature of the substrate, and it is not explicitly given there. Gorla and Gorla [27,38] considered a cylindrical geometry to represent the cornea; there was no noticeable effect of the substrate curvature and the constant substrate curvature does not in itself provide any driving force for fluid motion. It is generally assumed and accepted that the corneal shape is negligible in tear film dynamics. As a result, theoretical articles typically consider a flat substrate and use Cartesian coordinates based on that flat substrate to develop models for the tear film; we refer to this as the flat cornea approximation. Two points make the justification for the flat cornea approximation in tear film dynamics worth reconsidering. First, the cornea is a prolate spheroid to a good approximation ([45–47] and references therein), and this means that the curvature variation of the substrate may induce a pressure gradient in a thin film which is a driving mechanism for fluid motion. Second, in a recent assessment of the experimental measurements of tear film thinning in the central cornea by King-Smith et al. [48], there appeared to be significantly more thinning than expected based on surface tension-driven lubrication flows. In King-Smith et al. [48], interferometry was employed to measure the thickness of the tear film, and the rate of thinning was on the order of microns per minute. Several possible contributions for this rate of thinning were considered: flow along the cornea from surface tension due to film thickness variation, flow into the corneal surface, evaporation, and flow driven by the shape of the corneal surface. The first effect was eliminated because it cannot cause a net decrease in film thickness over a wide area during the time interval of interest, about 2–15 s after a blink. The second effect was eliminated because, if anything, we would expect flow to come into the tear film from the cornea. For the last effect, we estimated an initial thinning rate due to the pressure gradient induced by the prolate spheroidal corneal surface, and found that its contribution to the thinning caused by this effect was more than an order of magnitude smaller than the measured values. Thus, evaporation was thought to be the main contribution to the thinning by a process of elimination. We now return to the contribution due to the curvature of the prolate spheroidal shape of the cornea in an effort to more completely evaluate its role in tear film thinning.

For this study, we combine a number of tear film properties with the substrate shape. Tear fluid is weakly shear thinning, well described by a Cross model [49] according to Tiffany [16]. We choose to incorporate this property

into the study via the Ellis model [50], which is more shear-thinning than the Cross model but is easier to treat mathematically. The Ellis model's viscosity thins to zero as the shear stress increases, while the Cross model thins to a finite viscosity (often called the high shear rate plateau, which is roughly that of water for the tear film). Our model thus overestimates the effect of shear thinning and, in that respect, our results may be considered to place an upper bound on the contribution of shear thinning by emphasizing this effect more than in real tear fluid (because the viscosity is lower than in the Cross model at larger shear rates). We choose this bounding case to give shear thinning every chance to contribute to the dynamics in this model, and because the model allows us to write simple analytic forms for the equations governing the dynamics of a thin fluid film [50]. As an alternative, we also consider a Newtonian model with the viscosity chosen as the large shear rate limiting value [16].

During the writing of this article, a model of the creation and relaxation of a tear film using an Ellis fluid has appeared [28]. In that article, Jossic et al. used parameters that were fit to tear fluid properties at the lower end of the shear thinning range for the Ellis fluid. With respect to previous study on tear film formation and drainage [30,33,34,39,40], this article extends the rheological behavior to be closer to real eye properties [16]. However, they used a stress-free surface which neglects shear or any effect of the surfactants in the lipid layer (e.g., [21,22,34,48]). They used their model to optimize eye drop properties to make the tear film as uniform as they could.

We consider two cases in this article. One will have no meniscus, so that the eyelid margins are not mimicked, and will consist of covering half of a prolate spheroid with a thin film. The other will be half of a prolate spheroid or less, together with an axisymmetric meniscus that approximates the eyelid margins. The former will take into account the corneal shape alone; the latter combines the effect of corneal shape with an exaggerated effect of the eyelid margins.

Our lubrication models are based mainly on two previous studies. For the half prolate spheroid geometry, we follow the approach of Howell [51]. In that article, the varying size of the curvature of the substrate relative to the thin film surface is explored; the relevant case for us is the large curvature case where the dynamics of the thin film are dominated by the substrate curvature. We apply that approach to a new geometry and with new fluid properties. However, the large curvature limit results in a hyperbolic partial differential equation (PDE) for the film thickness whose solution characteristics do not allow one to apply boundary conditions such as film thickness and flux at a boundary (here, the eyelid); we find it useful to employ the approach of Roy et al. [52] in this latter case. They retain additional terms in the normal stress boundary condition and obtain a higher-order parabolic PDE more typical of lubrication approximations to the thin film dynamics. We apply this approach to a new substrate geometry to evaluate the influence of the cornea's shape together with that from the eyelids.

2 Formulation

We approximate the cornea as a prolate spheroidal surface (e.g., [45–47] and references therein); a sketch is shown in Fig. 1. We use prolate spheroidal coordinates (μ, ν, ϕ); the coordinates are given by

$$x' = c \sinh\mu \sin\nu \cos\phi, \quad y' = c \sinh\mu \sin\nu \sin\phi, \quad \text{and} \quad z' = c \cosh\mu \cos\nu. \tag{1}$$

Primes denote dimensional Cartesian variables; c is dimensional as well. Here $\pm c$ locates the foci of the elliptical cross section of the constant μ surface at a distance c from the origin along the z' axis; μ acts as a radius-like coordinate by changing the ellipticity while keeping those foci fixed. The polar angle ν has the range $0 \le \nu \le \pi$, and the azimuthal angle ϕ has the range $0 \le \phi < 2\pi$; however, we consider only the axisymmetric case, and so all quantities will be independent of ϕ. In our model, we will treat the film over the range $0 \le \nu \le \pi/2$ (or smaller) and $\mu_0 \le \mu \le \mu_0 + h'(\nu, t')/L$, where $h'(\nu, t')$ is the dimensional film thickness, and L is the length scale along the film.

We assume axisymmetry about the major axis of the prolate spheroid (that is, $\nu = 0$); the resulting eye shape is greatly simplified, but we hope to capture the essential behavior near the center of the cornea and to emphasize the role of substrate geometry. Corneal measurements [46] show that, in the (r', z')-plane, the cross section of the corneal surface is closely approximated by the sharp end of the ellipse given by

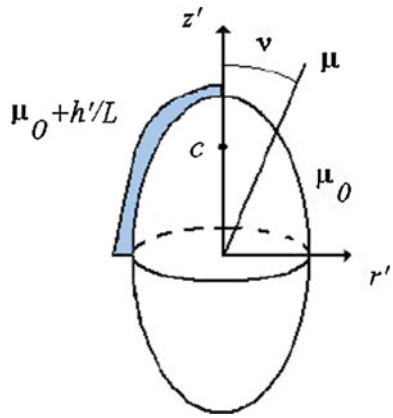

Fig. 1 Sketch of film cross section on a prolate spheroid; a cross section of the upper half of the film is shown (*shaded*). The surface $\mu = \mu_0$ is the constant μ surface that represents the corneal surface. As a visual aid, the radial and axial coordinates from a cylindrical coordinate system, r' and z' respectively, are shown. Foci for the elliptical cross section at $\mu = \mu_0$ are located at $z' = \pm c$. The "sharp" end is a good approximation to the cornea's shape [45–47]; the center of the cornea corresponds to the top of the prolate spheroid (at $\nu = 0$)

$$\left(\frac{r'}{b}\right)^2 + \left(\frac{z'}{a}\right)^2 = 1.$$

Using the parameters of Carney et al. [46], we write $a = R/(1+Q)$ and $b = R/\sqrt{1+Q}$; let $c = \sqrt{a^2 - b^2}$. Fitting the sharp end of the ellipse to corneal measurements determines representative values of $Q = -0.19$ and $R = 0.0078$ m [45]; alternatively, $a = 0.0096$ and $b = 0.0087$ m. The particular value of μ_0 we use for the cornea is given by $z' = a = c\cosh\mu_0$ for $\nu = 0$; rearranging gives $\mu_0 = \operatorname{arccosh}(1/\sqrt{-Q}) = 1.4722$ and $c = 0.0042$ m. The ellipticity of the corneal surface is given by $e = 1/\cosh\mu_0 = \sqrt{-Q} \approx 0.436$. Nondimensionalizing with c locates the foci $z = \pm 1$, and is relevant for eyes because it is quite close to the half width of a typical eye opening.

We shall assume two main geometries for the prolate spheroid. First, the upper half will be used; the equator at $\nu = \pi/2$ will be a symmetry boundary (a plane). Second, we shorten the domain in ν and apply a meniscus to mimic the effect of the lid margins. In the latter case, the effects of the prolate spheroidal substrate and of the meniscus at the lid margin are promoted beyond that in the human eye. Thus, this last choice is a bounding case for the drainage on the cornea in the following sense: if it is not important in this case, then we believe that it will not be important in the human eye.

The ratio of the representative film thickness d to the length scale along the film L is $d/L \ll 1$; this small value allows us to use lubrication theory to derive a PDE for the film thickness on the corneal surface. Following Howell [51], we choose scales based on Newtonian surface tension-driven flow and the zero shear rate viscosity η_0. Lengths along the film are chosen to be $L = c = 4.2$ mm based on Read et al. [45]; with this choice, the radius of curvature of the substrate and the length scale along the film are the same. The representative film thickness is chosen to be $d = 5\mu$m; thus, $\epsilon = d/L \approx 1.2 \times 10^{-3}$ in this article.

Dimensionless surface quantities required will include the scale factors relating distance to coordinate increments for the prolate spheroidal coordinates, with $\mathrm{d}s^2 = a_\nu^2\,\mathrm{d}\nu^2 + a_\phi^2\,\mathrm{d}\phi^2$, namely

$$a_\nu = N = [\sinh^2(\mu_0) + \sin^2(\nu)]^{1/2} \quad \text{and} \quad a_\phi = \sinh(\mu_0)\sin(\nu). \tag{2}$$

The principal curvatures may be written as

$$k_\nu = -N^{-3}\cosh\mu_0\sinh\mu_0 \quad \text{and} \quad k_\phi = -N^{-1}\coth\mu_0; \tag{3}$$

combinations of those quantities needed are

$$k_1 = k_\nu + k_\phi, \quad k_2 = k_\nu^2 + k_\phi^2 \quad \text{and} \quad k_3 = k_\nu k_\phi. \tag{4}$$

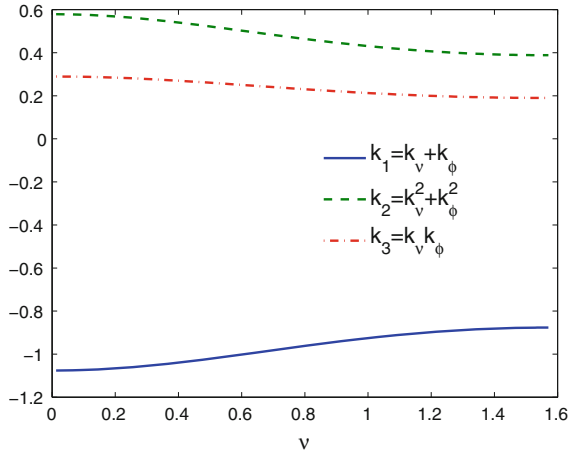

Fig. 2 Surface curvature quantities on the prolate spheroid representing the cornea. Here and throughout this article, $\mu_0 \approx 1.4722$; this value matches the shape found by Read et al. [45]

These quantities are $O(1)$ and, they vary by about 10% over the domain (see Fig. 2); this is sufficient to make the curvature of the substrate much more important in determining the film dynamics than the curvature variation due to changes in the film thickness [51].

The characteristic speed is $U = \sigma\epsilon^2/\eta_0$, where σ is the (assumed constant) surface tension of the tear–air interface, and η_0 is the zero-shear rate viscosity of tear fluid. The time t' is made dimensionless via $t' = (L/U)t$. The film thickness is made dimensionless with the typical thickness d via $h' = hd$. The coordinate outward from the prolate spheroidal surface is $\mu = \mu_0 + \epsilon\tilde{\mu}$; the coordinate $\tilde{\mu}$ is the nondimensional distance out from the $\mu = \mu_0$ surface, with the tear film in the interval $0 \le \tilde{\mu} \le h(\nu, t)$. The remaining dependent variables are nondimensionalized as follows:

$$u'_\mu = \epsilon U u_\mu, \quad u'_\nu = U u_\nu, \quad p' = \frac{\sigma}{L} p. \tag{5}$$

Here u_μ and u_ν are velocity components, p is the pressure. After nondimensionalization, we have at leading order for conservation of mass and momentum,

$$\frac{1}{\sin\nu}\frac{\partial}{\partial\nu}(u_\nu \sin\nu) + \frac{\partial u_\mu}{\partial\tilde{\mu}} = 0, \tag{6}$$

$$\frac{\partial}{\partial\tilde{\mu}}\left[\eta\frac{\partial u_\nu}{\partial\tilde{\mu}}\right] - \frac{1}{N}\frac{\partial p}{\partial\nu} = 0, \tag{7}$$

$$\frac{\partial p}{\partial\tilde{\mu}} = 0. \tag{8}$$

To obtain these equations, we require that the reduced Reynolds number be small, $\epsilon^2\rho U L/\eta_0 \ll 1$. The shear-rate-dependent viscosity $\eta = \eta(\partial u_\nu/\partial\tilde{\mu})$ will be discussed below (see (12)).

On the corneal surface $\tilde{\mu} = 0$, we assume no slip and impermeability $u_\mu = u_\nu = 0$.

On the free surface $\tilde{\mu} = h(\nu, t)$, we have the kinematic condition for the axisymmetric case

$$\frac{\partial h}{\partial t} = u_\mu - \frac{u_\nu}{a_\nu}\frac{\partial h}{\partial\nu}, \tag{9}$$

and the stress conditions. We use the normal stress condition from Roy et al. [52],

$$p = -\tilde{k} \quad \text{with } \tilde{k} = k_1 + \epsilon\left(k_2 h + \nabla_s^2 h\right). \tag{10}$$

For the tangential stress condition on the free surface $\tilde{\mu} = h$, two limiting cases may replace the action of the polar lipids and other surfactants present in tears. In the limit where a surfactant has a strong effect, the free surface is rendered immobile to leading order [53]; this is the tangentially immobile limit. When the effect of surfactants on

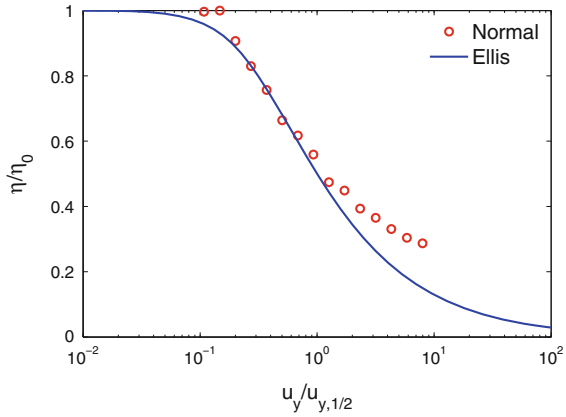

Fig. 3 Ellis fluid behavior used in this article for fitting tears. We choose $\alpha = 3$ to get $-2/3$ decay. To graphically match tears, we chose $\dot{\gamma}_{1/2} = 20\ \mathrm{s}^{-1}$ and $\eta_0 = 5 \times 10^{-3}$ Pa s; the latter parameter is from Tiffany [16]. The data points are viscosity values from Tiffany [16]; "Normal" indicates that the measurements are for healthy tears from normal subjects (as opposed to those with dry eye)

the tear film is assumed to be weak, then the surface is very mobile and may be thought of as clean to leading order; this is the stress-free limit. In this article, we use the stress-free condition

$$\frac{\partial u_\nu}{\partial \tilde{\mu}} = 0 \tag{11}$$

because it promotes faster drainage of the film, and is thus consistent with the approach of bounding the film behavior with modeling choices that accelerate drainage (the tangentially immobile case was estimated in King-Smith et al. [6]). Terms of $O(\epsilon)$, including those in (10), are retained in the approach of Roy et al. [52], while those terms are neglected in Howell [51]; for a complete discussion, see the latter.

We bound the shear thinning by replacing the Cross model [49], which decreases to finite viscosity at large shear rates with a $-2/3$ power for tears [16], with the Ellis constitutive relation (e.g., [50]), which decays to zero viscosity at large shear rates. The nondimensional viscosity is given by

$$\eta = \frac{1}{1+\beta\,|\tau|^{\alpha-1}}, \quad \tau = \eta\frac{\partial u_\nu}{\partial \tilde{\mu}}, \quad \text{and} \quad \beta = \left(\frac{\eta_0 U/d}{\tau_{1/2}}\right)^{\alpha-1}, \tag{12}$$

where $\tau_{1/2}$ is a material parameter (see Appendix A). We choose the parameter $\alpha = 3$ so that the decay of the viscosity is still a $-2/3$ power for large shear (derivation not shown), and we graphically fit the beginning of the decay to tear film data as shown in Fig. 3. To do this, we use the simplification of lubrication theory to write $\tau_{1/2} = (\eta_0/2)(\dot{\gamma}_{1/2})$; then with our choice of velocity scale, we have $\beta = [(2\sigma\epsilon^2)/(\mathrm{d}\eta_0\dot{\gamma}_{1/2})]^{\alpha-1}$. Substitution of our choice of $\dot{\gamma}_{1/2}$ and the other tear film parameters results in $\beta \approx 0.065$. In what follows, we will use this estimate to describe tear film quantities, but we will also vary β over a wide range to find interesting mathematical behavior.

Applying Howell's approach [51] to our geometry and incorporating the Ellis fluid, the substrate curvature dominates the flow of the thin fluid film. For the tear film thickness, we obtain

$$\frac{\partial h}{\partial t} + \frac{1}{\sin(\nu)N}\frac{\partial}{\partial \nu}\left[\frac{\sin\nu}{N}\frac{h^3}{3}\frac{\partial k_1}{\partial \nu} + \beta\frac{\sin\nu}{N^\alpha}\frac{h^{\alpha+2}}{\alpha+2}\left|\frac{\partial k_1}{\partial \nu}\right|^{\alpha-1}\frac{\partial k_1}{\partial \nu}\right] = 0; \tag{13}$$

details may be found in Appendix B. Note that $\partial k_1/\partial \nu \geq 0$ for the prolate spheroids that we study, so that we may ignore the absolute value in the above equation and use

$$\frac{\partial h}{\partial t} + \frac{1}{\sin(\nu)N}\frac{\partial}{\partial \nu}\left[\frac{\sin\nu}{N}\frac{h^3}{3}\frac{\partial k_1}{\partial \nu} + \beta\frac{\sin\nu}{N^\alpha}\frac{h^{\alpha+2}}{\alpha+2}\left(\frac{\partial k_1}{\partial \nu}\right)^\alpha\right] = 0. \tag{14}$$

Since $\partial k_1/\partial \nu \geq 0$, the curvature gradient is a driving force for removal of fluid from the region near $\nu = 0$. The term proportional to β represents shear thinning effects; when $\beta = 0$, we recover the Newtonian result.

We write Eq. 14 as

$$a_\nu a_\phi\frac{\partial h}{\partial t} + \frac{\partial}{\partial \nu}\left[\frac{a_\phi}{a_\nu}\frac{h^3}{3}\frac{\partial k_1}{\partial \nu} + \beta\frac{a_\phi}{a_\nu^\alpha}\frac{h^{\alpha+2}}{\alpha+2}\left(\frac{\partial k_1}{\partial \nu}\right)^\alpha\right] = 0. \tag{15}$$

We refer to this equation as the large curvature limit. This PDE is first order in space and is thus hyperbolic. The characteristics of the solution are such that no boundary conditions may be specified, except for symmetry that is compatible with the substrate's prolate spheroidal shape; symmetry requires that odd spatial derivatives of h are set to zero at $\nu = 0$ and $\nu = \pi/2$. We do this in subsequent numerical solutions for this equation, and inspection of the characteristics will confirm this assertion (e.g., in Fig. 8).

Retaining $O(\epsilon)$ terms in the film's momentum equation and in the stress conditions at the free surface yields a fourth-order PDE for the free surface $h(\nu, t)$; this case is discussed in Sect. 3.2 for a Newtonian fluid.

3 Results

3.1 Large curvature limit

In this section, we study the equations in the large curvature limit.

3.1.1 Central cornea thinning

We first estimate the initial thinning rate of the precorneal tear film at the center of the cornea located at $\nu = 0$. We consider only half of a prolate spheroid about the plane of symmetry $\nu = \pi/2$. Consider Newtonian flow with a stress-free surface; the PDE for the film thickness dynamics is

$$\frac{\partial h}{\partial t} = -\frac{1}{N \sin\nu}\frac{\partial}{\partial \nu}\left(\frac{h^3}{3}\frac{\sin\nu}{N}\frac{\partial k_1}{\partial \nu}\right). \tag{16}$$

Letting $h(\nu, 0) = h_0(\nu) = 1$, and evaluating the substrate curvature derivatives at $\nu = 0$, yields, in dimensional terms,

$$\frac{\partial h'}{\partial t'}(\nu = 0, t = 0) = \frac{8\sigma}{3\eta_0}\frac{Q[h'(0,0)]^3}{R^3}. \tag{17}$$

where the apical radius R and the asphericity Q are the parameters that define the prolate spheroidal shape of the cornea; as mentioned above, Read et al. [45] used corneal geometry measurements to find $R = 0.0078$ m and $Q = -0.19$. The properties of tear are chosen to be $\sigma = 0.045$N/m and $\eta_\infty = 10^{-3}$ Pa s after [17] and [16]. These values give $\partial h'/\partial t'(0, 0) = -0.072\,\mu$m/min; experimental values from King-Smith et al. [48] are, on the average about $-4\,\mu$m/min. Thus, the contribution from Newtonian flow at the center of the cornea is rather small compared to measured values. If we use $\eta_0 \to \eta_\infty \approx 10^{-3}$ Pa s, which is the high shear rate value for tears (roughly equal to the viscosity of water, as is commonly used in Newtonian studies [30,31,33,36,41]), we find a thinning rate of $0.36\,\mu$m/min at the center of the cornea, which is only 10% of the measured value. We note that this rate is four times that found in King-Smith et al. [6] where the tangentially immobile free surface was used.

If we consider the Ellis fluid, then there are additional terms present in the evolution of the thin film dynamics governed by (14). However, when evaluating an estimate of the initial thinning rate, symmetry eliminates any terms involving $(\partial k_1/\partial \nu)^\alpha$, and thus the shear thinning is eliminated at $\nu = 0$. The Ellis fluid thins at the same rate as a Newtonian fluid at $\nu = 0$.

This symmetry allows for a particulary simple solution for the thickness at $\nu = 0$; let $h(0, t) \equiv h_{\text{mid}}(t)$. Using the symmetry of this point, one finds that h_{mid} satisfies an ordinary differential equation, namely,

$$\frac{\mathrm{d}h_{\text{mid}}}{\mathrm{d}t} = -\frac{h_{\text{mid}}}{N^2(0)}\frac{\mathrm{d}^2 k_1(0)}{\mathrm{d}\nu^2}, \quad h_{\text{mid}}(0) = 1. \tag{18}$$

Solving the ODE, using the initial condition and evaluating the known expressions gives

$$h_{\text{mid}}(t) = \left[1 + \frac{2t}{N^2(0)}\frac{\mathrm{d}^2 k_1(0)}{\mathrm{d}\nu^2}\right]^{-1/2}, \tag{19}$$

or

$$h_{\text{mid}}(t) = \left[1 + \frac{8\cosh\mu_0}{\sinh^6\mu_0}t\right]^{-1/2} = \left[1 + \frac{8(-Q)^{5/2}}{(1+Q)^3}t\right]^{-1/2}. \tag{20}$$

Thus, the thickness never ruptures in finite time at $\nu = 0$; we shall see below that singularities will occur elsewhere in finite time.

We conclude that the initial tear film thinning rate caused by the shape of the cornea at its center is negligible under normal circumstances.

3.1.2 Numerical solutions

Our numerical computations use an implementation of the method of lines. We used a Chebyshev spectral discretization in space with Chebyshev points mapped to the interval $(-\pi/2 \le \nu \le \pi/2)$; only half of the standard domain is needed, $(0 \le \nu \le \pi/2)$. We avoid the singularity at the origin by choosing an even number of grid points; we also enforce symmetry about $\nu = 0$ in the differentiation matrices. The grid points for which solutions are shown are given by

$$\nu_j = -\frac{\pi}{2}\cos\left(\frac{j\pi}{N-1}\right), \quad j = \frac{N}{2}+1, \frac{N}{2}+2, \ldots, N-1. \tag{21}$$

For time stepping, we used `ode15s` in Matlab. Numerical experiments showed that 96–128 modes in $0 \le \nu \le \pi/2$ yielded solutions that were converged under grid refinement; we typically used 112 modes.

3.1.3 Newtonian viscosity

Results for a Newtonian fluid and large substrate curvature are shown in Fig. 4. In these results, we observed $t^{-1/2}$ thinning at $\nu = 0$ and what appears to be a finite time singularity at $\nu = \pi/2$. The computation was terminated at $t = 24$; $h(\pi/2, t)$ increases rapidly after this time. Both kinds of behavior were predicted by Howell [51] for Newtonian fluids in different geometries. The computed blow-up time from the method of characteristics (details below) is $t = 24.75$ which is shortly after the end of the computation. The spectral method we used is not well suited to shock capture, and so we rely on the analysis of the characteristics below for accurate values of the shock or singularity formation time.

3.1.4 Non-Newtonian viscosity

We next consider the Ellis fluid with boundary conditions $\partial h/\partial\nu(\pi/2, t) = 0$. For the properties of the tear fluid, we estimate that the shear thinning parameter is $\beta = 0.065$. This case appears to develop a finite-time singularity at $\nu = \pi/2$, and is difficult to distinguish from the Newtonian case. We conclude that there is no significant contribution to tear film thinning for parameters appropriate for that case.

Deviating from the tear film parameters, we increase β over orders of magnitude to explore the behavior of the equations. Choosing $\beta = 10^2$ gives the results shown in Fig. 5. The singularity in the solution occurs at finite time similar to the case of a Newtonian or weakly shear thinning fluid; however, the singularity is now a shock that occurs at $\nu_c < \pi/2$. The time t_c and location ν_c of the shock formation depend on β. Solutions for the film thickness at different times t_{end} prior to singularity formation for various values of β are shown in Fig. 6. The behavior appears to converge to shock formation at a particular time and place as $\beta \to \infty$. In this case, the limiting behavior of the fluid for $\beta \to \infty$ is a power law, and we analyze that case in Sect. 3.1.5.

We note that the shear rate at the wall, $\partial u_\nu/\partial\mu(\mu_0, \nu, t)$ varies with ν and t during the computations. The maximum value is typically ranges from 500 s^{-1} at $\nu \approx 0.6$ to about 300 s^{-1} at $\nu \approx 0.9$ as time increases. This is true for $0.065 \le \beta \le 1000$, and it occurs because the substrate curvature dominates the evolution for $0 \le \nu \le 1$, approximately. The shear rate appears to develop a jump in slope when a singularity forms. We note that these shear rates cause a small viscosity that occurs near the middle of the computational domain, and this viscosity is below

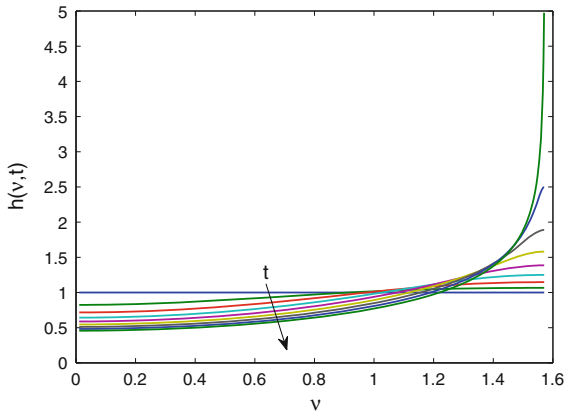

Fig. 4 Evolution from the initial condition $h(\nu, 0) = 1$ for a Newtonian fluid in the large curvature limit of Howell [51]. The *curves* shown are at $t = 0, 3, 6, \ldots, 24$

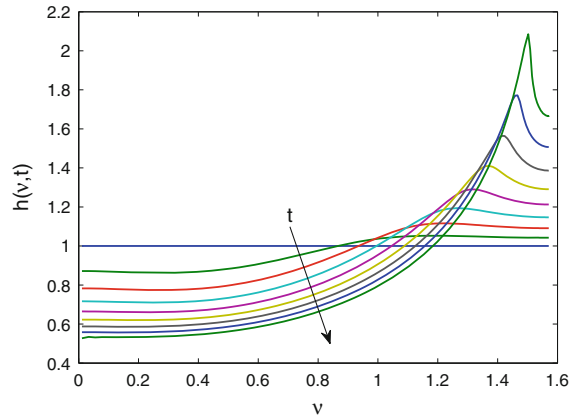

Fig. 5 $h(\nu, t)$ for an Ellis fluid with $\beta = 10^2$. The time to singularity formation is similar to $\beta = 0$, but the singularity is now a shock located at $\nu_s < \pi/2$. Solutions are shown for $t = 0, 2, 4, \ldots, 16$

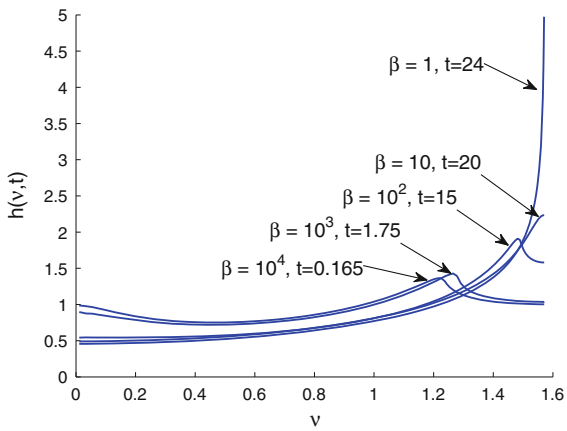

Fig. 6 $h(\nu, t_{\text{end}})$ for the Ellis fluid for several different β, and at times t_{end} close to blow-up or a shock. The time to blow-up or shock formation decreases with increasing β; the computation for each value of β is stopped prior to the singularity forming

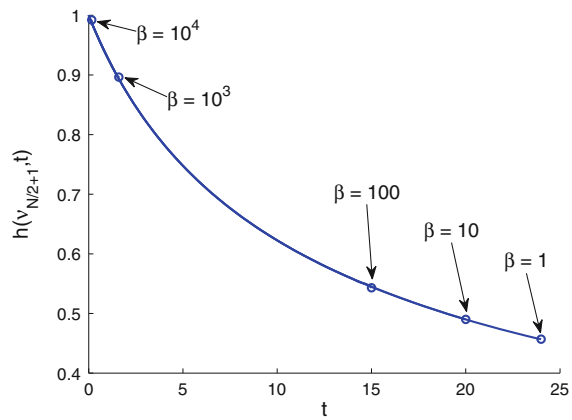

Fig. 7 Evolution of $h(\nu_1, t)$ for an Ellis fluid. This approximation to the central film thickness is apparently independent of β, as discussed in the text. The different end times t_{end} of the computations are indicated by the *circles*

the η_∞ that is essentially that of water for the Cross model [16]. Thus, this model does emphasize tear thinning more than real tear fluid.

For increasing β, shear thinning becomes more marked. But in our central corneal thinning rate estimate in Sect. 3.1.1, we found that the initial thinning rate at $\nu = 0$ is independent of the shear thinning term. We adjusted β over a wide range of values and found the thinning rate at the nearest grid point to the origin, $\nu_{N/2+1}$. Curves for various time intervals $0 \le t \le t_{\text{end}}$ prior to the singularity formation are shown in Fig. 7, and it is clear that the computed results are independent of β as well.

3.1.5 Shock formation

Define $q(\nu) = a_2(\nu)(\partial k_1/\partial \nu)/a_1(\nu)$; then we can write Eq. 15 as

$$a_\nu a_\phi \frac{\partial h}{\partial t} + \frac{\partial}{\partial \nu}\left[\frac{h^3}{3}q + \beta \frac{1}{a_\phi^{\alpha-1}} \frac{h^{\alpha+2}}{\alpha+2} q^\alpha\right] = 0 \tag{22}$$

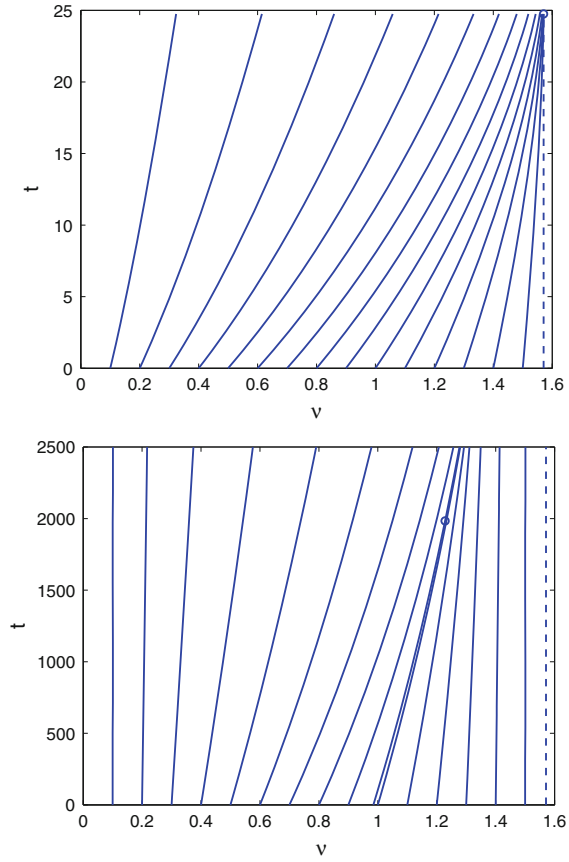

Fig. 8 *Top* Newtonian results ($\alpha = 1$) for characteristic curves with $h(\nu, 0) = 1$; the singularity forms at about $t_c \approx 24.75$ at $\nu = \pi/2$ as predicted by our application of Howell's theory [51] to this new geometry. *Bottom* The power law limit with $\alpha = 3$ and $\beta \to \infty$; the singularity forms from $s_c = 0.9847$, and the shock first forms at $\nu_c = 1.2284$ and $t_c = 1984$. The shock forms away from the symmetry plane for the shear thinning fluid

Now along a characteristic, we have

$$\frac{\mathrm{d}t}{\mathrm{d}\nu} = \frac{a_\nu(\nu)a_\phi(\nu)}{h^2(\nu)q(\nu) + \beta a_\phi^{1-\alpha}(\nu)h^{\alpha+1}(\nu)q^\alpha(\nu)}, \tag{23}$$

and Eq. 22 can then be integrated along a characteristic to yield $B(h, \nu) = B(h_0, s)$, where

$$B(h, \nu) = \frac{h^3}{3}q(\nu) + \beta a_\phi^{1-\alpha}(\nu)\frac{h^{\alpha+2}}{\alpha+2}q^\alpha(\nu), \tag{24}$$

s is the initial value of ν along the characteristic, and $h_0(s)$ the corresponding initial value of h. Specifically, we have

$$\frac{h^3(\nu)}{3}q(\nu) + \beta a_\phi^{1-\alpha}(\nu)\frac{h^{\alpha+2}(\nu)}{\alpha+2}q^\alpha(\nu) = \frac{h_0^3(s)}{3}q(s) + \beta a_\phi^{1-\alpha}(s)\frac{h_0^{\alpha+2}(s)}{\alpha+2}q^\alpha(s). \tag{25}$$

Combining (23) and (25) is not easily accomplished, particularly for general values of α; the ability to combine these easily and get analytical expressions for t was crucial for the success of the Newtonian case studied by Howell. If we consider the case for large β, we get a similar simplification.

For $\beta \gg 1$ and time rescaled with β, then to leading order we obtain

$$\frac{\mathrm{d}t}{\mathrm{d}\nu} = \frac{a_\nu(\nu)a_\phi(\nu)}{a_\phi^{1-\alpha}(\nu)h^{\alpha+1}(\nu)q^\alpha(\nu)}, \tag{26}$$

and

$$a_\phi^{1-\alpha}(\nu)h^{\alpha+2}(\nu)q^\alpha(\nu) = a_\phi^{1-\alpha}(s)h_0^{\alpha+2}(s)q^\alpha(s). \tag{27}$$

Table 1 Shock characteristic initial value s_c, shock formation time t_c and shock formation location ν_c for different values of α on this prolate spheroidal substrate with $\mu_0 = 1.4722$

α	1	1.5	2	3	4
s_c	1.5708	1.1941	1.0889	0.9847	0.92945
t_c	24.75	83.481	238.47	1984	17413
ν_c	1.5708	1.4963	1.3949	1.2284	1.1076

Note that the equations in this limit are the same as for a power law fluid. Using (27) to eliminate $h(\nu)$ from (26) leads to the desired simplification, namely,

$$\frac{\mathrm{d}t}{\mathrm{d}\nu} = \frac{a_\nu(\nu)a_\phi(\nu)}{\left[a_\phi^\omega(\nu)q^{1-\delta-\omega}(\nu)\right]\left[a_\phi^\omega(s)h^{\alpha+1}(s)q^{\alpha\delta}(s)\right]}, \tag{28}$$

where

$$\gamma = \frac{\alpha^2-1}{\alpha+2}, \quad \delta = \frac{\alpha+1}{\alpha+2}, \quad \omega = \frac{1-\alpha}{\alpha+2}. \tag{29}$$

Integration yields

$$th_0^{\alpha+1}(s)a_\phi^{-\gamma}(s)q^{\alpha\delta}(s) = \int_s^\nu a_\nu(\xi)a_\phi^{\alpha-\gamma}(\xi)q^{\alpha(\delta-1)}(\xi)\mathrm{d}\xi. \tag{30}$$

A shock forms where the characteristics first cross, that is, where $\mathrm{d}t/\mathrm{d}s = 0$. Solving (30) and its derivative with respect to s simultaneously yields

$$t_c = \frac{-(\alpha+2)a_\nu a_\phi^\alpha}{\alpha(\alpha+1)q^{\alpha-1}\dot{q}\left(1-\frac{\alpha-1}{\alpha}\frac{q}{\dot{q}}\frac{\dot{a}_\phi}{a_\phi}\right)}. \tag{31}$$

where the dot indicates differentiation with respect to s. The location where $(\mathrm{d}t/\mathrm{d}\nu)|_{\nu=s} = 0$ gives the initial value for the characteristic on which the shock first appears, s_c. If we choose $\alpha = 1$, then we recover the Newtonian case given by Howell [51] as his Eq. 36. For $\alpha = 3$, we find

$$t_c = \frac{-5a_\nu a_\phi^3}{12q^2\dot{q}\left(1-\frac{2}{3}\frac{q}{\dot{q}}\frac{\dot{a}_\phi}{a_\phi}\right)}. \tag{32}$$

The characteristics in the (ν, t) for $\alpha = 1$ and 3 are shown in Fig. 8.

Solving differential equation (28) subject to the initial condition $\nu(0) = s_c$ for $0 \le t \le t_c$ gives the location where the shock first forms, ν_c. When $\alpha = 3$, the shock first forms at $\nu_c = 1.2284$ and $t_c = 1984$, approximately, as indicated by the circle in the bottom plot of Fig. 8. Results for different α are summarized in Table 1. These results agree well with the computed film profiles in Fig. 6; the location of the steepening computed from the hyperbolic PDE for the film surface is consistent with the theoretical predictions from the equations for the characteristics.

3.2 Keeping higher-order terms

In this section, we consider the approximation of Roy et al. [52]. In this approximation, we return to the Newtonian fluid, and $O(\epsilon)$ terms are kept from the normal stress boundary conditions and in momentum conservation in the ν direction. With the estimated size of $\beta \approx 0.065$ for tears, and the contribution from shear thinning only becoming significant when about three orders of magnitude larger in the other model, we choose to neglect shear thinning in this model and to use η_∞ as a characteristic viscosity in order to bound the motion with a low value. Thus, for this model, we shall only consider a Newtonian tear film on a prolate spheroidal substrate.

Applying the results of Roy et al. [52], the normal stress boundary condition is then

$$p = -k_1 - \epsilon \left\{ hk_2 + \frac{1}{N \sin \nu} \frac{\partial}{\partial \nu} \left[\frac{\sin \nu}{N} \frac{\partial h}{\partial \nu} \right] \right\}, \tag{33}$$

and one must compute the $O(\epsilon)$ term in the ν-momentum equation and the stress-free boundary condition on h. We find that combining the first two orders and evaluating their result for our prolate spheroidal coordinate system gives

$$\frac{\partial \zeta}{\partial t} + \frac{1}{\sin(\nu) N} \frac{\partial}{\partial \nu} \left(\frac{h^2 \zeta}{3} \frac{\sin \nu}{N} \frac{\partial \tilde{k}}{\partial \nu} \right) = 0, \quad \zeta = h - \epsilon \frac{k_1}{2} h^2 + \epsilon^2 \frac{k_3}{3} h^3, \tag{34}$$

where $\tilde{k}$ is given by (10). In this case, we compute solutions on $0 < \nu < \nu_e$, with $\nu_e \leq \pi/2$. The same Chebyshev spectral method is applied to this problem as in the large curvature equation. Because the equation is now fourth order in space, we must specify more boundary conditions. We gain the ability to specify a meniscus, however; this is important in attempting to model the tear film.

We consider two different choices for the boundary and initial condition. First, we consider an initially uniform film ($h(\nu, 0) = 1$) with symmetry conditions ($\partial h/\partial \nu = \partial^3 h/\partial \nu^3 = 0$) at each end of the interval. Results are shown in Fig. 9. In this case, the higher-order terms prevent finite-time blow-up that occurs in the hyperbolic equation for the prolate spheroidal case in this study and from Howell [51] for different geometries, which is not unexpected. The thinning rate at $\nu = 0$ is quite similar to that of the large curvature limit.

We now turn to the second combination of initial and boundary conditions. We still enforce symmetry at $\nu = 0$, but we impose $h = h_0 = 13$ [54] and no flux at the other end of the domain (either $\nu = \pi/2$ or $\pi/4$). The initial condition in this case is $h(\nu, 0) = 1 + (h_0 - 1)(\nu/\nu_e)^m$; we typically chose $m = 16$. The film thickness at the boundary $h_0 = 13$ corresponds to 65 μm, and the thickness of the meniscus decreases to the nominal film thicknesses between 5 μm and about 1 mm in our computations; the ratio of length scales is still small.

Results for both interval sizes are shown in Figs. 10 and 11. The earlier times are plotted with solid curves; at those times, a very small amount of fluid has moved to the meniscus region, but a thin region is developing as the low-pressure meniscus (with a region of positive curvature enforced from the boundary) collects fluid. At later times, the film distributions with the dashed curves show that the meniscus is larger after collecting fluid from the rest of the film. When $\nu_e = \pi/2$, the meniscus there does not have a strong influence on the thickness evolution at $\nu = 0$. There is some oscillation in the film thickness in the region connecting the meniscus with the rest of the film; this is not uncommon in coating or draining flows (e.g., [36]). When $\nu_e = \pi/4$, there is some visible influence on $h(0, t)$, though it is not large. The time scale is about 100 s, and so the time to decrease from 5 μm to about 1.25 μm as in Fig. 11 is about 24 nondimensional time units, or more than 2hrs dimensionally. This is clearly much too slow compared to the 4 μm/min observed experimentally [48]. For $p = 16$ and $\nu_e = \pi/6$, $h(\nu_{N/2+1}, 24) = 0.854$, though there is not monotonic decay in time to this value. Thus, simply shortening the domain does not necessarily continue to accelerate the thinning rate at $\nu = 0$. We conclude that the thinning due to the substrate curvature together with the meniscus is insufficient to make a significant contribution to central corneal thinning rates for physiological times.

4 Discussion and conclusion

Based on an estimate for the thinning rate at the center of the cornea, for both Newtonian or Ellis fluids, the effect of the cornea's prolate spheroidal shape is not important when compared with typical tear film thinning rates that are measured in vivo. The Ellis fluid made no difference at the center of the cornea in the large curvature limit because the shear thinning terms vanished by symmetry at the $\nu = 0$ stagnation point. These results appear to fit well with the conclusions of King-Smith et al. [48]. They measured the decrease in thickness as a function of time following a blink in a central region of the cornea, and they considered the time interval from roughly 2–15 s after a blink. Thinning rates on the order of 4 μm/min were found in that study. They hypothesized that the thinning of

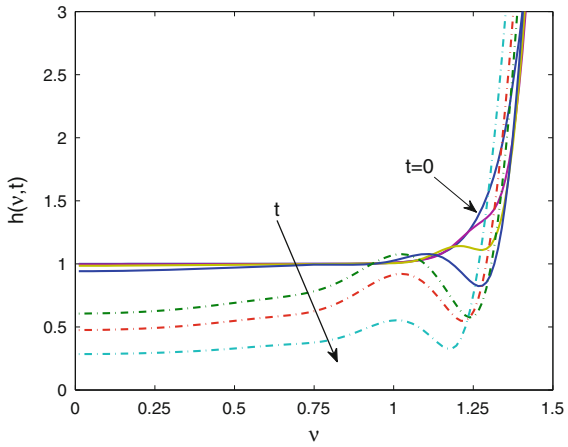

Fig. 9 Evolution from $h(\nu, 0) = 1$ for Newtonian fluid up to $t = 24$ for the Roy et al. model applied to our geometry. Compare these results with Fig. 4

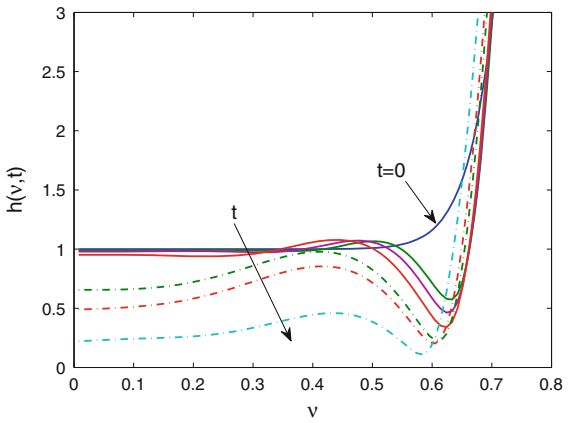

Fig. 10 Evolution from $h(\nu, 0) = 1$ for Newtonian fluid up to $t = 24$ for the Roy et al. model. Compare these results with Fig. 4

Fig. 11 Same as Fig. 10 except the domain being now $0 < \nu < \pi/4$. The film thickness at the center of the cornea is less at the end of the computation; in dimensional form, the thickness is about 1 μm after about 40 min

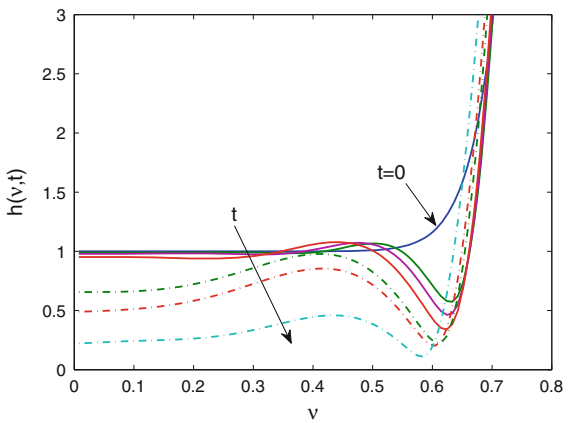

the tear film could be caused by one of three things: (1) inward flow into the cornea; (2) tangential flow along the corneal surface due to either Marangoni effect or capillary forces; or (3) mass loss due to evaporation. Most authors believe that flow into the cornea is in fact outward due to an increase in osmolarity in the tear film. Regarding tangential flow, there is certainly an upward motion of the tear film for 1–2 s following a blink [6,21,22,34], but this motion dies out to low levels rapidly thereafter, and does not appear to be responsible for the thinning of the tear film observed in experiment. Regarding flows driven by capillarity and the variation of the tear film thickness, they appear to be too slow to be significant in this time interval [48] away from localized regions of thinning driven by the meniscus near the lid margins (the so-called black lines in the literature) [29–32,36]. For the experiments of King-Smith et al. [48], it thus appears that evaporation is an important contribution to the thinning rate of the tear film on the cornea. In any case, the contribution to film thinning due to the prolate spheroid shape appears to be at most 2–10% of the measured values of the thinning rate from King-Smith et al. [48]. In King-Smith et al. [6], the initial thinning rate at the center of the cornea for the tangentially immobile case was estimated as in Sect. 3.1.1, and an initial rate of $-0.09\,\mu$m/min was found. In this article, our stress-free boundary condition resulted in faster initial thinning rate estimates. We note that the magnitude of the thinning rate measured experimentally depends on the method used [55,56], but we believe that our conclusion is robust.

Taking license with the shear thinning parameters, we found that the type and location of the singularity that occurs in the large curvature limit differs from that of the Newtonian case considered by Howell [51]. In the Newtonian case, finite time blow-up occurs on the equator ($\nu = \pi/2$) which is the location of maximum curvature of the substrate (that is, where k_1 is least negative; see Fig. 2). When an Ellis fluid is used, the singularity is modified to a shock that forms at a value of $\nu < \pi/2$ when β (i.e., the shear thinning) is large enough. We used the method of characteristics to locate the first formation of the shock; our direct numerical method to solve the PDE for the tear film thickness is not well suited to shock capture. As the shear thinning increases, the shock formation is faster, and the location is farther from the equator.

We then studied a Newtonian fluid model proposed by Roy et al. [52] with menisci incorporated into the computation to mimic (and exaggerate) the effect of the eyelid margins. We moved the edge of the computational domain closer to the center of the eye to increase the effect of the meniscus, so that it could cooperate with the pressure gradient due to the corneal shape. We still found that the thinning rate was not significant enough to warrant including the effect of the cornea shape when compared to measured thinning rates. The distribution of tear fluid is modified somewhat from the flat cornea approximation; the tear film does not develop a parabolic cap in the middle because the substrate curvature variation generates a pressure gradient to drain the fluid from the middle regions far from the meniscus.

It may be possible in some combination of conditions and/or for some subjects that the corneal shape may affect the tear film thinning rate on the cornea. For example, if evaporation were essentially halted by humidity and an unusually effective lipid layer, then the thinning rate of the tear film could have some significant contribution from the corneal shape. However, in the typical case, the corneal shape may be neglected as a cause for tear film thinning in comparison to other contributions.

Future study of mathematical interest could include studying different ellipsoidal geometries (not just prolate spheroids) and the stability of the flow on such ellipsoids, which would require relaxing the axisymmetry assumption.

Acknowledgments This material based upon this study is supported by the National Science Foundation under Grant Nos. 0616483 and 1022706. R.J.B. thanks H. Abelman for helpful discussion and the Institute for Mathematics and Its Application, University of Minnesota, for its hospitality and support during this project. R.U. thanks the Department of Mathematical Sciences, University of Delaware for its support and hospitality while on sabbatical leave there.

Appendix A: Conservation equations and prolate spheroidal coordinates

Mass is conserved for the incompressible fluids of this study by making the flows divergence free:

$$\nabla' \cdot \mathbf{u}' = 0. \tag{35}$$

Momentum is conserved via

$$\rho\left(\frac{\partial \mathbf{u}'}{\partial t'} + \mathbf{u}' \cdot \nabla' \mathbf{u}'\right) = \nabla' \cdot \mathbf{T}' - \nabla' p' \tag{36}$$

where τ' is the dynamic stress tensor. For the Newtonian fluid, we have

$$\tau' = \eta 2\mathbf{E}' \quad \text{and} \quad 2\mathbf{E}' = \left[\nabla' \mathbf{u}' + \left(\nabla' \mathbf{u}'\right)^T\right]; \tag{37}$$

in this case, the viscosity η is constant and, in the stress, it multiplies the usual rate of strain tensor. For the Ellis fluid in simple shear flow, the viscosity is a function of the second invariant of the dynamic stress tensor II_τ, namely [57,58],

$$\eta' = \frac{\eta_0}{1 + \left(\sqrt{|II_\tau|}/\tau_{1/2}\right)^{\alpha-1}}. \tag{38}$$

The zero shear rate viscosity η_0, the characteristic shear stress magnitude $\tau_{1/2}$ to reach $\eta = \eta_0/2$ and the exponent α are material parameters. The invariant in the Ellis viscosity expression is given by [57,58]

$$II_\tau = [\mathrm{tr}(\tau)]^2 - \mathrm{tr}(\tau^2). \tag{39}$$

Note that we have made a particular choice for the constant and exponents appearing in the form given by Macosko [58, p. 86], after Myers [50], for example. The stress components have been related to the rate-of-strain components for power law fluids in Perazzo and Gratton [59].

Equations (35)–(39) are non-dimensionalized using

$$t = \frac{t'\sigma}{\eta_0 d}, \quad u_\nu = \frac{\epsilon^3 u'_\nu}{U}, \quad u_\phi = \frac{\epsilon^3 u'_\phi}{U}, \quad u_\mu = \frac{\epsilon^4 u'_\mu}{U}, \quad p = \frac{p'\epsilon^2 L}{\sigma}, \quad \tau = \frac{\epsilon^3 L}{\sigma}\tau' \tag{40}$$

where $U = \dfrac{\epsilon^2\sigma}{\eta_0}$ and $Re = \dfrac{\sigma\rho d}{\eta_0^2}$ is the Reynolds number. The equations become

$$\frac{\partial}{\partial\nu}\left(a_\phi u_\nu\right) + \frac{\partial}{\partial\phi}\left(a_\nu u_\phi\right) + \frac{\partial}{\partial\mu}\left(a_\phi a_\nu u_\mu\right) = 0, \tag{41}$$

and

$$Re\left(\frac{\partial\mathbf{u}}{\partial t} + \mathbf{u}\cdot\nabla\mathbf{u}\right) = \nabla\cdot(\eta 2\mathbf{E}) - \nabla p. \tag{42}$$

Here

$$\nabla p = \frac{\epsilon}{a_\nu}\frac{\partial p}{\partial\nu}\hat{\mathbf{e}}_\nu + \frac{\epsilon}{a_\phi}\frac{\partial p}{\partial\phi}\hat{\mathbf{e}}_\phi + \frac{\partial p}{\partial\mu}\hat{\mathbf{e}}_\mu \tag{43}$$

and the convective terms are

$$\begin{aligned}\mathbf{u}\cdot\nabla\mathbf{u} = \mathbf{e}_\mu &\left[(\mathbf{u}\cdot\nabla)u_\mu - \frac{u_\phi^2}{\sqrt{\sinh^2\mu+\sin^2\nu}}\frac{\cosh\mu}{\sinh\mu} + \frac{u_\mu u_\nu\cos\nu\,\sin\nu}{[\sinh^2\mu+\sin^2\nu]^{3/2}} - \frac{u_\nu^2\cosh\mu\,\sinh\mu}{\left(\sinh^2\mu+\sin^2\nu\right)^{3/2}}\right]\\ + \mathbf{e}_\nu &\left[(\mathbf{u}\cdot\nabla)u_\nu - \frac{u_\phi^2}{\sqrt{\sinh^2\mu+\sin^2\nu}}\frac{\cos\nu}{\sin\nu} - \frac{u_\mu^2\cos\nu\,\sin\nu}{\left(\sinh^2\mu+\sin^2\nu\right)^{3/2}} + \frac{u_\mu u_\nu\cosh\mu\,\sinh\mu}{\left(\sinh^2\mu+\sin^2\nu\right)^{3/2}}\right]\\ + \mathbf{e}_\phi &\left[(\mathbf{u}\cdot\nabla)u_\phi + \frac{u_\phi}{\sqrt{\sinh^2\mu+\sin^2\nu}}\left(\frac{\cosh\mu}{\sinh\mu}u_\mu + \frac{\cos\nu}{\sin\nu}u_\nu\right)\right],\end{aligned} \tag{44}$$

where, for a scalar function $f = f(\mu,\nu,\phi)$,

$$(\mathbf{u}\cdot\nabla)f = \frac{u_\mu}{\sqrt{\sinh^2\mu+\sin^2\nu}}\frac{\partial f}{\partial\mu} + \frac{u_\nu}{\sqrt{\sinh^2\mu+\sin^2\nu}}\frac{\partial f}{\partial\nu} + \frac{u_\phi}{\sinh\mu\,\sin\nu}\frac{\partial f}{\partial\phi}. \tag{45}$$

The rate of strain tensor is the symmetric part of $\nabla\mathbf{u}$ and has components

$$\mathbf{E}_{\mu\mu} = \frac{1}{\sqrt{\sinh^2\mu+\sin^2\nu}}\frac{\partial u_\mu}{\partial\mu} + \frac{\cos\nu\,\sin\nu}{\left[\sinh^2\mu+\sin^2\nu\right]^{3/2}}u_\nu, \tag{46}$$

$$\mathbf{E}_{\nu\nu} = \frac{1}{\sqrt{\sinh^2\mu+\sin^2\nu}}\frac{\partial u_\nu}{\partial\nu} + \frac{\cosh\mu\,\sinh\mu}{\left[\sinh^2\mu+\sin^2\nu\right]^{3/2}}u_\mu, \tag{47}$$

$$\mathbf{E}_{\phi\phi} = \frac{1}{\sinh\mu\,\sin\nu}\frac{\partial u_\phi}{\partial\phi} + \frac{1}{\sqrt{\sinh^2\mu+\sin^2\nu}}\left(\frac{\cosh\mu}{\sinh\mu}u_\mu + \frac{\cos\nu}{\sin\nu}u_\nu\right), \tag{48}$$

$$\begin{aligned}\mathbf{E}_{\mu\nu} = &\frac{1/2}{\sqrt{\sinh^2\mu+\sin^2\nu}}\left(\frac{\partial u_\nu}{\partial\mu} + \frac{\partial u_\mu}{\partial\nu}\right)\\ &- \frac{1/2}{[\sinh^2\mu+\sin^2\nu]^{3/2}}\left(\cos\nu\,\sin\nu\,u_\mu + \cosh\mu\,\sinh\mu\,u_\nu\right),\end{aligned} \tag{49}$$

$$\mathbf{E}_{\mu\phi} = \frac{1/2}{\sinh\mu\,\sin\nu}\frac{\partial u_\mu}{\partial\phi} + \frac{1/2}{\sqrt{\sinh^2\mu+\sin^2\nu}}\frac{\partial u_\phi}{\partial\mu} - \frac{1/2}{\sqrt{\sinh^2\mu+\sin^2\nu}}\frac{\cosh\mu}{\sinh\mu}u_\phi, \tag{50}$$

$$\mathbf{E}_{\nu\phi} = \frac{1/2}{\sinh\mu\,\sin\nu}\frac{\partial u_\nu}{\partial\phi} + \frac{1/2}{\sqrt{\sinh^2\mu+\sin^2\nu}}\frac{\partial u_\phi}{\partial\nu} - \frac{1/2}{\sqrt{\sinh^2\mu+\sin^2\nu}}\frac{\cos\nu}{\sin\nu}u_\phi, \tag{51}$$

For a Newtonian fluid, the viscous terms are given by

$$\nabla\cdot(2\mathbf{E}) = \frac{1}{a_\nu a_\phi}\left[\epsilon^2\frac{\partial}{\partial\nu}\left(\frac{a_\phi}{a_\nu}\frac{\partial}{\partial\nu}\right)+\epsilon^2\frac{\partial}{\partial\phi}\left(\frac{a_\nu}{a_\phi}\frac{\partial}{\partial\phi}\right)+\frac{\partial}{\partial\mu}\left(a_\nu a_\phi\frac{\partial}{\partial\mu}\right)\right]\left[\epsilon u_\nu\hat{\mathbf{e}}_\nu+\epsilon u_\phi\hat{\mathbf{e}}_\phi+\epsilon^2 u_\mu\hat{\mathbf{e}}_\mu\right] \tag{52}$$

For the Ellis fluid, we require the viscous terms to be $\nabla\cdot(2\eta\mathbf{E})$, with η a function of the shear stress as indicated above.

The boundary conditions are, on $\mu=\mu_0$,

$$u_\nu = u_\phi = u_\mu = 0, \tag{53}$$

and on $\mu=\mu_0+\epsilon h(\nu,\phi,t)$,

$$\frac{\partial u_\nu}{\partial\mu}+\epsilon k_\nu u_\nu = 0, \tag{54}$$

$$\frac{\partial h}{\partial t} = u_\mu - \frac{u_\nu}{a_\nu}\frac{\partial h}{\partial\nu}-\frac{u_\phi}{a_\phi}\frac{\partial h}{\partial\phi}, \tag{55}$$

and

$$p = -k_1-\epsilon k_2\eta-\epsilon\nabla^2 h+O(\epsilon^2), \tag{56}$$

where $k_1=k_\nu+k_\phi$ and $k_2=k_\nu^2+k_\phi^2$.

Appendix B: Ellis fluid

Here, we give details for the Ellis fluid at leading order for large substrate curvature assuming axisymmetric behavior. Inside the film $0<\tilde{\mu}<h(\nu,t)$ where $\mu=\mu_0+\epsilon\tilde{\mu}$, the leading order equations are

$$\frac{1}{\sin\nu}\frac{\partial}{\partial\nu}(u_\nu\sin\nu)+\frac{\partial u_\mu}{\partial\tilde{\mu}} = 0, \tag{57}$$

$$\frac{\partial}{\partial\tilde{\mu}}\left(\eta\frac{\partial u_\nu}{\partial\tilde{\mu}}\right) = \frac{1}{N}\frac{\partial p}{\partial\nu}, \tag{58}$$

$$\frac{\partial p}{\partial\tilde{\mu}} = 0. \tag{59}$$

On the substrate $\tilde{\mu}=0$, we still have $u_\nu=u_\mu=0$. On the free surface, $\tilde{\mu}=h(\nu,t)$, we have at leading order

$$\frac{\partial h}{\partial t} = u_\mu - \frac{u_\nu}{a_\nu}\frac{\partial h}{\partial\nu}, \tag{60}$$

$$p = -k_1, \tag{61}$$

$$\frac{\partial u_\nu}{\partial\tilde{\mu}} = 0. \tag{62}$$

The Ellis constitutive relation to leading order is

$$\eta = \frac{1}{1+\beta\left|\partial u_\nu/\partial\tilde{\mu}\right|^{\alpha-1}}. \tag{63}$$

Integrating (58) once and applying (62) gives

$$\eta\frac{\partial u_\nu}{\partial\tilde{\mu}} = -\frac{1}{N}\frac{\partial p}{\partial\nu}(h-\tilde{\mu}). \tag{64}$$

Manipulating the constitutive relations gives

$$\frac{\partial u_\nu}{\partial\tilde{\mu}} = \eta\frac{\partial u_\nu}{\partial\tilde{\mu}}+\beta\left|\eta\frac{\partial u_\nu}{\partial\tilde{\mu}}\right|^{\alpha-1}\eta\frac{\partial u_\nu}{\partial\tilde{\mu}}. \tag{65}$$

Combining these last equations, integrating $d\tilde{\mu}$, and using the no-slip boundary condition gives

$$u_\nu = \frac{1}{2N}\frac{\partial p}{\partial \nu}\left[(h-\tilde{\mu})^2 - h^2\right] + \beta\lambda^{\alpha-1}\left(\frac{-1}{N}\frac{\partial p}{\partial \nu}\right)^{\alpha}\frac{h^{\alpha+1}-(h-\tilde{\mu})^{\alpha+1}}{\alpha+1}. \tag{66}$$

Integrating across the film thickness yields the flux:

$$q = \frac{-1}{N}\frac{\partial p}{\partial \nu}\frac{h^3}{3} - \beta\left|\frac{-1}{N}\frac{\partial p}{\partial \nu}\right|^{\alpha-1}\frac{1}{N}\frac{\partial p}{\partial \nu}\frac{h^{\alpha+2}}{\alpha+2}. \tag{67}$$

Using the leading-order normal stress boundary condition introduces twice the mean substrate curvature; since the substrate curvature is non-decreasing, we can eliminate the absolute value and we obtain

$$q = \frac{1}{N}\frac{\partial k_1}{\partial \nu}\frac{h^3}{3} + \beta\left(\frac{1}{N}\frac{\partial k_1}{\partial \nu}\right)^{\alpha}\frac{h^{\alpha+2}}{\alpha+2}. \tag{68}$$

Using the flux together with conservation of mass inside the film and the kinematic condition for the free surface yields the evolution Eq. 14 for h in the large curvature limit.

References

1. Holly FJ, Lemp MA (1977) Tear physiology and dry eyes. Rev Surv Ophthalmol 22:69–87
2. Mishima S (1965) Some physiological aspects of the precorneal tear film. Arch Ophthalmol 73:233–241
3. Ehlers N (1965) The precorneal film: biomicroscopical, histological and chemical investigations. Acta Ophthalmol Suppl 81:3–135
4. Norn MS (1979) Semiquantitative interference study of fatty layer of precorneal film. Acta Ophthalmol 57:766–774
5. Bron AJ, Tiffany JM, Gouveia SM, Yokoi N, Voon LW (2004) Functional aspects of the tear film lipid layer. Exp Eye Res 78: 347–360
6. King-Smith PE, Fink BA, Nichols JJ, Nichols KK, Braun RJ, McFadden GB (2009) The contribution of lipid layer movement to tear film thinning and breakup. Investig Ophthalmol Vis Sci 50:2747–2756
7. Chen H-B, Yamabayashi S, Ou B, Tanaka Y, Ohno S (1997) Structure and composition of rat precorneal tear film: a study by in vivo cryofixation. Investig Ophthalmol Vis Sci 38:381–387
8. Gipson IK (2004) Distribution of mucins at the ocular surface. Exp Eye Res 78:379–388
9. Govindarajan B, Gipson IK (2010) Membrane-tethered mucins have multiple functions on the ocular surface. Exp Eye Res 90: 655–663
10. King-Smith PE, Fink BA, Hill RM, Koelling KW, Tiffany JM (2004) The thickness of the tear film. Curr Eye Res 29:357–368
11. King-Smith PE, Fink BA, Nichols JJ, Nichols KK, Hill RM (2006) The thickness of the human precorneal tear film: evidence from reflection spectra. J Opt Soc Am A 23:2097–2104
12. Wang J, Fonn D, Simpson TL, Jones L (2003) Precorneal and pre- and postlens tear film thickness measured indirectly with optical coherence tomography. Investig Ophthalmol Vis Sci 44:2524–2528
13. Palakuru JR, Wang J, Aquavella JV (2007) Effect of blinking on tear dynamics. Investig Ophthalmol Vis Sci 48:3032–3037
14. Johnson ME, Murphy PJ (2006) Temporal changes in the tear menisci following a blink. Exp Eye Res 83:517–525
15. Harrison WW, Begley CG, Lui H, Chen M, Garcia M, Smith JA (2008) Menisci and fullness of the blink in dry eye. Optom Vis Sci 85:706–714
16. Tiffany JM (1991) The viscosity of human tears. Int Ophthalmol 15:371–376
17. Pandit JC, Nagyová B, Bron AJ, Tiffany JM (1999) Physical properties of stimulated and unstimulated tears. Exp Eye Res 68: 247–253
18. Leiske DL, Raju SR, Ketelson HA, Millar TJ, Fuller GG (2010) The interfacial viscoelastic properties and structures of human and animal meibomian lipids. Exp Eye Res 90:598–604
19. McCulley JP, Shine W (1997) A compositional based model for the tear film lipid layer. Trans Am Ophthalmol Soc XCV:79–93
20. Nagyová B, Tiffany JM (1999) Components of tears responsible for surface tension. Curr Eye Res 19:4–11
21. Berger RE, Corrsin S (1974) A surface tension gradient mechanism for driving the pre-corneal tear film after a blink. J Biomech 7:225–238
22. Owens H, Phillips J (2001) Spread of the tears after a blink: velocity and stabilization time in healthy eyes. Cornea 20:484–487
23. Mudgil P, Torres M, Millar TJ (2006) Adsorption of lysozyme to phospholipid and meibomian lipid monolayer films. Colloids Surf B 48:128–137
24. Mudgil P, Millar TJ (2008) Adsorption of apo- and holo-tear lipocalin to a bovine meibomian lipid film. Exp Eye Res 86:622–628
25. Zhang L, Matar OK, Craster RV (2003) Analysis of tear film rupture: effect of non-Newtonian rheology. J Colloids Interface Sci 262:130–148
26. Zhang L, Matar OK, Craster RV (2004) Rupture analysis of the corneal mucus layer of the tear film. Mol Simul 30:167–172

27. Gorla MSR, Gorla RSR (2004) Rheological effects of tear film rupture. Int J Fluid Mech Res 31:552–562
28. Jossic L, Lefevre P, de Loubens C, Magnin A, Corre C (2009) The fluid mechanics of shear-thinning tear substitutes. J Non-Newton Fluid Mech 161:1–9
29. McDonald JE, Brubaker S (1971) Meniscus-induced thinning of tear films. Am J Ophthalmol 72:139–146
30. Wong H, Fatt I, Radke CJ (1996) Deposition and thinning of the human tear film. J Colloid Interface Sci 184:44–51
31. Sharma A, Tiwari S, Khanna R, Tiffany JM (1998) Hydrodynamics of meniscus-induced thinning of the tear film. In: Sullivan DA, Dartt DA, Meneray MA (eds) Lacrimal gland, tear film, and dry eye syndromes, vol 2. Plenum, New York pp 425–431
32. Miller KL, Polse KA, Radke CJ (2002) Black line formation and the "perched" human tear film. Curr Eye Res 25:155–162
33. Jones MB, Please CP, McElwain DLS, Fulford GR, Roberts AP, Collins MJ (2005) Dynamics of tear film deposition and drainage. Math Med Biol 22:265–288
34. Jones MB, McElwain DLS, Fulford GR, Collins MJ, Roberts AP (2006) The effect of the lipid layer on tear film behavior. Bull Math Biol 68:1355–1381
35. Aydemir E, Breward CJW, Witelski TP (2011) The effect of polar lipids on tear film dynamics. Bull Math Biol 73:1171–1201
36. Braun RJ, Fitt AD (2003) Modelling precorneal tear film drainage after a blink. Math Med Biol 20:1–28
37. Winter KN, Anderson DM, Braun RJ (2010) A model for wetting and evaporation of a post-blink precorneal tear film. Math Med Biol 27:211–225
38. Gorla MSR, Gorla RSR (2000) Nonlinear theory of tear film rupture. J Biomech Eng 122:498–503
39. Braun RJ, King-Smith PE (2007) Model problems for the tear film in a blink cycle: single equation models. J Fluid Mech 586: 465–490
40. Heryudono A, Braun RJ, Driscoll TA, Cook LP, Maki KL, King-Smith PE (2007) Single-equation models for the tear film in a blink cycle: realistic lid motion. Math Med Biol 24:347–377
41. Maki KL, Braun RJ, Driscoll TA, King-Smith PE (2008) An overset grid method for the study of reflex tearing. Math Med Biol 25:187–214
42. Maki KL, Braun RJ, Ucciferro P, Henshaw WD, King-Smith PE (2010) Tear film dynamics on an eye-shaped domain II. Flux boundary conditions. J Fluid Mech 647:361–390
43. Maki KL, Braun RJ, Henshaw WD, King-Smith PE (2010) Tear film dynamics on an eye-shaped domain I. Pressure boundary conditions. Math Med Biol 27:227–254
44. Berger RE (1973) Pre-corneal tear film mechanics and the contact lens. Dissertation, Johns Hopkins University
45. Read SA, Collins MJ, Carney LG, Franklin RJ (2006) The topography of the central and peripheral cornea. Investig Ophthalmol Vis Sci 47:1404–1415
46. Carney LG, Mainstone JC, Henderson BA (1997) Corneal topography and myopia: a cross-sectional study. Investig Ophthalmol Vis Sci 38:311–320
47. Harris WF (2006) Curvature of ellipsoids and other surfaces. Ophthalmic Physiol Opt 26:497–501
48. King-Smith PE, Nichols JJ, Nichols KK, Fink BA, Braun RJ (2008) Contributions of evaporation and other mechanisms to tear film thinning and breakup. Optom Vis Sci 85:623–630
49. Cross MM (1965) Rheology of non-Newtonian fluids: a new flow equation for pseudoplastic systems. J Colloid Interface Sci 20:417–437
50. Myers TG (2005) Application of non-Newtonian models to thin film flow. Phys Rev E 72:066302
51. Howell PD (2003) Surface-tension-driven flow on a moving curved surface. J Eng Math 45:283–308
52. Roy RV, Roberts AJ, Simpson ME (2002) A lubrication model of coating flows over a curved substrate in space. J Fluid Mech 454:235–261
53. Naire S, Braun RJ, Snow SA (2000) Limiting cases of gravitational drainage of a vertical free film for evaluating surfactants. SIAM J Appl Math 61:889–913
54. Golding TR, Bruce AS, Mainstone JC (1997) Relationship between tear-meniscus parameters and tear-film breakup. Cornea 16:649–661
55. Tomlinson A, Doane MG, McFadyen A (2009) Inputs and outputs of the lacrimal system: review of production and evaporative loss. Ocul Surf 7:17–29
56. Kimball SH, King-Smith PE, Nichols JJ (2010) Evidence for the major contribution of evaporation to tear film thinning between blinks. Investig Ophthalmol Vis Sci 51:6294–6297
57. Bird RB, Armstrong RC, Hassager O (1987) Dynamics of polymeric fluids. Vol I–fluid mechanics. Wiley, New York
58. Macosko CW (1994) Rheology: principles, measurements and applications. Wiley, New York
59. Perazzo CA, Gratton J (2003) Thin film of non-Newtonian fluid on an incline. Phys Rev E 67:016307